Electrodynamics in Iron and Steel

John Paul Wallace
Casting Analysis Corp.
(Dated: 12 January 2009)

Abstract

In order to calculate the reflected EM fields at low amplitudes in iron and steel, more must be understood about the nature of long wavelength excitations in these metals. A bulk piece of iron is a very complex material with microstructure, a split band structure, magnetic domains and crystallographic textures that effect domain orientation. Probing iron and other bulk ferromagnetic materials with weak reflected and transmitted inductive low frequency fields is easy to perform but the responses are difficult to interpret because of the complexity and variety of the structures effected by the fields. First starting with a simple single coil induction measurement and classical EM calculation to show the error is grossly under estimating the response. Extending this experiment to measuring the transmission of the induced fields allows the extraction of three dispersion curves which define these internal fields. One dispersion curve spanning the frequency range of measurements had an exceedingly small effective mass of 2.56×10^{-39}kg ($2.7 \times 10^{-9} m_e$) for those spin waves. Using a time dependent field to lift the phase degeneracy for a select population of spin waves leads to a reduction in their effective mass by ten orders of magnitude, which is just a reflection of the size of the coherent state. These experiments taken together display the characteristics of a high temperature Bose-Einstein like condensation (BELC) can be initiated by pumping and then actively dominates the field induction measurements of iron and steel well past the Curie temperature. First presented single sensor and high temperature transmission data as, Crystals for a Spin Wave Amplifier, at 20th Conference of Crystal growth and Epitaxy, AACGE/West,6 June 2006, Fallen Leaf Lake, California.

INTRODUCTION

This review of old data covers some neglected physics in the interpretation of low frequency reflection and transmission of weak inductive fields in ferromagnetic materials. Historically these experimental effects are not new and have been detected and reported as anomalously large permeability measurements of ferromagnetic material by a time dependent technique introduced by H. Rowland(1) in 1873 using a pair of inductors coupled by a ferromagnetic torus. Extending the technique to high temperature measurements of iron in 1910 by E.M. Terry(2) and measurements in high purity iron by R.M. Borzoth(3) 1937 produced values for permeability orders of magnitude greater than statically determined values. The details of the magnetic domain motion in the ferromagnetic torus were examined in 1949(4). The application of Ampere's law assuming no internal sources of time dependent fields other than the source inductor was the basis of this transformer design and application. Here a simplified form of this measurement is considered for isolating the material contributions to the responses that are not otherwise described by Ampere's law.

In addition, to my own problem of satisfactorily calibrating induction measurements on iron and steel to detect defects there is a set of other unanswered questions. The storage mechanisms involved in the operation of ferro resonant load leveling transformer patented by J. Sola(5) in 1954 require a more detailed explanation. The anomalous eddy current loss(6) which is a large effect for induction heating in Fe and FeSi alloys also has not been accurately described. Also the steel corrosion inspection method "remote field testing" using slowly propagating, highly insensitive long range fields in low carbon steels(7) also requires an explanation. These unsolved problems coupled with the large conflict in the simplest experimental field reflection data to classical calculated values for ferromagnetic materials exhibits a weakness in our understanding. Ferromagnetism is a quantum mechanical phenomena, but a macroscopic connection to the field equations of Maxwell is essential to usefully solving induction measurement problems. Since the time of Roland's introduction of the coupled transformer experiment, microscopic theories of elementary spin excitations have been developed to describe the temperature dependence of magnetization. The question of how a slowly varying time dependent induction $\mathbf{H}(t)$ interacts with individual spins, spin waves and structures such as magnetic domain boundaries (MDB) in iron and steel to produce the measured responses has remained an open question.

Spin wave theory developed as a lattice theory starting with considerations of the mechanics of a single one dimensional array of spins(8,9). These early works form the basis for the extensive investigations that have continued to the present. One difficulty in the application of a lattice theory to iron is that it does not include the local lattice relaxation dependence to the magnetization. This is a large effect in iron and can be seen in the fitted plot of lattice parameter as a function of temperature(10) through the Curie point in figure 1. In this plot the linear expansion with temperature is removed so the non linear response of the lattice to temperature variations taken through the Curie point become evident. The strains associated with the material below the curie point are significant.

Spin waves and photons are the bosons that allow an exchange of spin states between carriers in ferromagnetic metal such as iron. These exchanges in addition to the transport of carriers are how the spin system is modified by the application of external fields and induced currents. These two classes of effects in addition to the lattice relaxation determines the measured responses and the various ways in which energy is distributed or escapes from the metal. Non saturated soft ferromagnets that will be considered are partitioned by an array

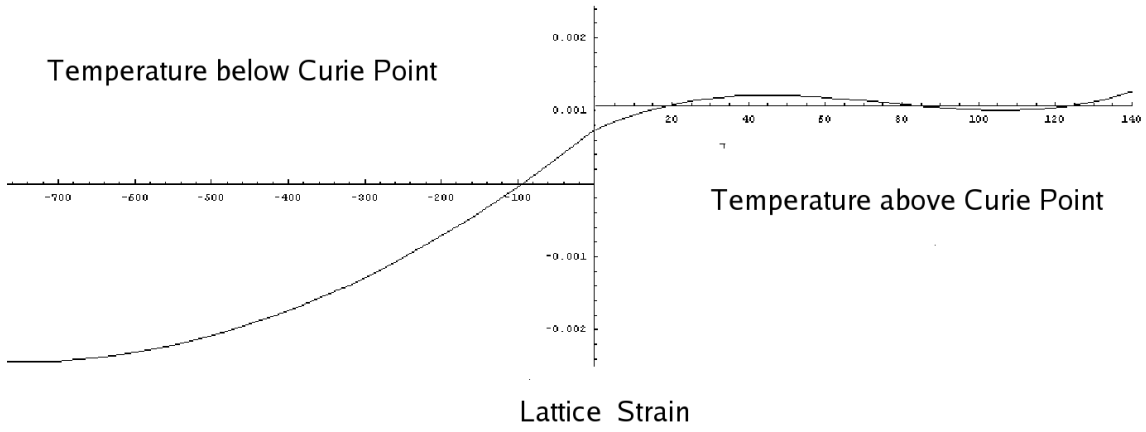

FIG. 1: **Lattice parameter variations reduced from powder x-ray lattice parameter data for iron as a function of temperature with the linear response removed. The temperatures are referenced from the Curie point. The displacements are in angstroms with the lattice parameter of iron being 2.86 angstroms at 30^oC. The curve is similar to the saturation magnetization as a function of temperature. Has a total equivalent strain at low temperatures of about .1% deviating from the extended high temperature linear lattice parameter verses temperature.**

of MDB and the coupling between these regions will control the propagation of long range fields through the bulk of the sample. This couplings can be summaries in the first table.

Table 1: Field and Current Couplings

Region	Coupling	Details
bulk	strain or phonon	no direct coherent coupling to spin wave
bulk	current	$\mathbf{j} \times \mathbf{m}$ spin wave generation
bulk	$\mathbf{H}(\omega)$	lifts phase degeneracy $\mathbf{q}(\omega)$ spin waves
MDB	current	electron transport across **MDB** generate spin waves
MDB	spin wave	emission and capture across **MDB** move **MDB**
MDB	photon	emission and capture across **MDB** move **MDB**

In iron these 6 process are active at once. Iron's split band structure(11) allows for direct transitions between electronic spin states, that are not available in the other ferromagnetic transition metals and provides another source for non thermal spin waves. Not included is the spin wave terminating at a free surface generating a photon.

ANALYSIS IN WEAK FIELDS

The construction of the Rowland transformer is too complex to allow a simple closed form analysis to represent the experiment. You have to eliminate the bends to get a simple experimental apparatus with a source inductor around a cylinder and a receiving inductor

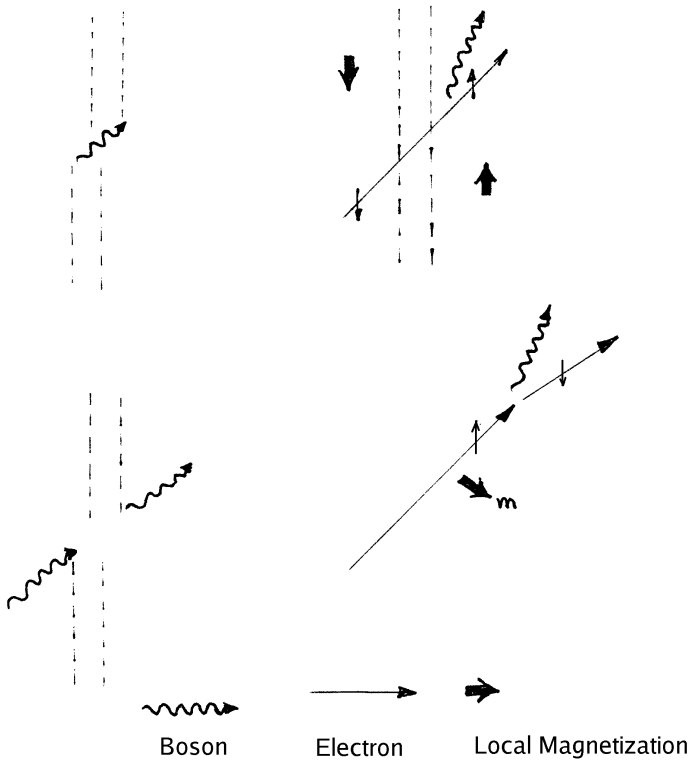

FIG. 2: **Graphic of the principal transitions that can generate a non thermal boson population. The magnetic domain boundaries are shown as double broken parallel lines. The electrons crossing the domain boundaries carry a spin state that will suffer a change in energy after traveling through a domain boundary.**

either being the same inductor, figure 3a, or a displaced inductor, figure 3b. These geometries allows the EM boundary value problem to be easily solved in closed form using only assumptions of material homogeneity.

Our first measurements are for weak time dependent fields with long free space wavelengths that will act as a small perturbation on iron's spin system. For the applied induction field interacting with a ferromagnetic conductor there are three regions in the material that influence the interaction. The first is a near surface where some domain motion is inhibited by the effect of the surface to minimize leakage fields. The next deeper region penetrated by the induction field can drive domain motion more easily. Finally there is the bulk interior below the electromagnetic skin depth where any measurable transverse propagating fields vanish.

All the measurements described are macroscopic measurements on physically large samples when compared to grain size, electronic mean free path and the conductors electromagnetic skin depths. These measurements are on a small scale when compared to free space electromagnetic wavelengths and acoustical wavelengths of the fields at the applied frequency.

The measurements made here will represent one of a set of experiments that will isolate the non classical effects that are common and easily detectable at low levels with low

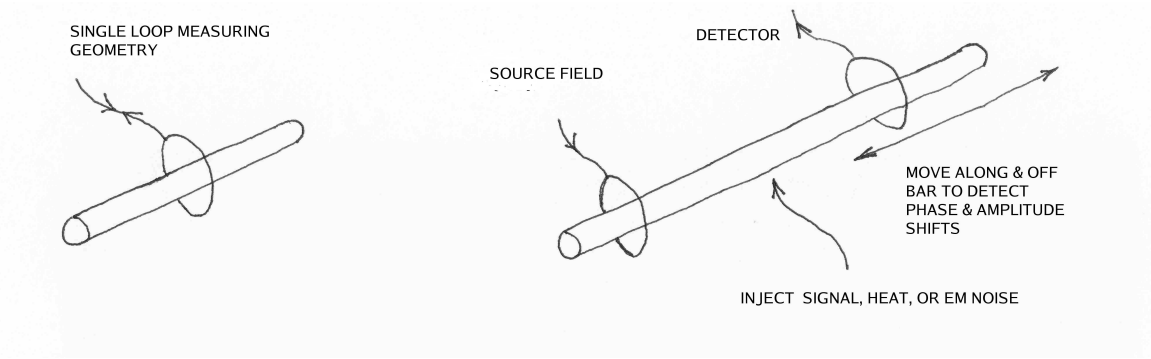

FIG. 3: **a) Single sensor encircling , b) Dual coil transmission measurement with possible second source injection.**

frequency, time-dependent fields that interact with ferromagnetic conductors and insulators.

CALIBRATION OF INDUCTION MEASUREMENTS

The principle technique used here is often referred to AC magnetic susceptibility measurements and this is a label which is misleading. For simple conductors the technique is very powerful and accurate in reducing measured reflections to structural and electrical conductivity profiles. For magnetic material this technique must assume a magnetic constitutive relation that may not be accurate or adequate. Therefore, these measurements will simply be called induction measurements with an analysis based on a macroscopic set of Maxwell's equations.

An induction measurement system consists of two parts. A network that supplies and detects the field and the sensor which is usually a coil. This coupled system is calibrated as a complete system. The calibration requires the measurement of a standard of know properties in a computable boundary value geometry that reduces the standard to a calculable response. The electromagnetic induction scattering problem as a boundary value problem was solved exactly in closed form for selected geometries by Dodd and Deeds(12) in the low frequency range below 10 Mhz for typical metallic conductors. In the quasi-static approximation for conductivity these solutions are accurate for simple conductors such as copper, where the electronic mean free path is short relative to the structure of the sample being measured(13). This allowed induction measurement of non ferromagnetic conductors to produce precise dimensional and conductivity measurements at ambient(14) and at high temperatures.

What follows is a simple calibration scheme for the fields which can be though of as an analog to optical reflection. In order, to do induction studies of high temperature materials, crystal growth processes a simple calibration technique was introduced(15) where a known conductivity standard is compared to an unknown sample. Calibration was reduced to practice when complex arithmetic could be done on a microprocessor(16) to allow the mapping of a signal space into a measurement space. This essentially removes the details of the network that connected the source and receivers so long as they are operated in a linear response region well below any self resonance of the measurement system. This in effect removes the measurement system by the calibration in using a two dimensional transformation matrix for each frequency of measurement. Extending this calibrated measurement technique to ferromagnetic systems such a carbon steels, pure iron, cast irons, ferromagnetic

ore bodies, ferromagnetic amorphous metals, ferro fluids and composite ferromagnetic material produces results that conflict with simple magnetic models. The assumption required for electrical conduction analysis is quasi-static approximation and with ferromagnetic material this assumption is insufficient. The quasi-static approximation for electron scattering in conduction does not have an analogue when considering a system of ferromagnetic spins and their response to a time dependent field.

For example the simple geometry, figure 3, of measurement and analysis is a single turn induction loop used both as a source and receiver surrounding a right circular cylinder of copper or a well annealed iron. Solving the boundary value problem of the wave equation for the vector potential, $\mathbf{A}$, in a source free region such as the interior of a conductor will yield the local electric and magnetic fields through the vector potential. The field equation in the source free region where we have used the definition $\mathbf{B} = \mu\mathbf{H}$ is simply:

$$\nabla^2\mathbf{A} - \sigma\mu\frac{\partial\mathbf{A}}{\partial t} - \epsilon\mu\frac{\partial^2\mathbf{A}}{\partial t^2} = 0 \qquad [1]$$

This above expression is easily solved by maintaining the continuity of both the electric field, $\mathbf{E}$ and the magnetic induction, $\mathbf{H}$, at each boundary for either one or two dimensions with multiple layers.

The known properties of the measurement are the signal level, frequencies, the diameter of the loop inductor and the diameter of the bars under test. If a conductor of known purity, dimension and temperature is used as a standard one can capture the complex signal as reflected from this standard $S_m = (x_m, y_m)$ and also compute the reflected response, $S_c = (x_c, y_c)$. The computed value of the reflection is found by solving the boundary value problem. One can compute a 2×2 matrix $\mathbf{T}$, that connects these two vectors.

$$S_c = \mathbf{T}S_m \qquad [2]$$

A simple example with the source normalized to $S_{source} = (1, 0)$, then a perfect conductor filling an encircling loop will produce a response of $S_c(\sigma \to \infty) = (-1, 0)$ and for an empty sensor $S_c = (0, 0)$. For subsequent measurements, S_m, the application of the matrix $\mathbf{T}$, transfers the signal vector into a space that can be interpreted, R.

$$R = \mathbf{T}S_m \qquad [3]$$

It is useful to consider the limits of these measurements and responses in a simple experiment. With fixed coil or loop surrounding a cylindrical conductor the response $R(\sigma)$ where σ is the conductivity will obey this relationship,

$$K = \frac{|R(\sigma)|}{|R(\sigma \to \infty)|} < 1 \qquad [4]$$

This can be shown by solving the boundary value problem and observing the behavior of the responses by taking the cylinder's conductivity to infinity. This is simple to show either for a long encircling coil about a cylinder, a plane wave on an infinite plane reflector or a single loop surrounding a cylinder. Similarly if the material permeability is examined in the same way the result are the same. There can be no measured reflected signal that was greater than initially supplied. This is easy to prove in any geometry. This is because the propagation vector in the material contains a product of σ and μ and even if complex the limiting relations of equation 4 and 5 remain true.

$$\frac{|R(\sigma,\mu)|}{|R(\sigma\to\infty,\mu_o)|}\leq 1 \qquad [5]$$

An example of this type of computation for a simple one dimensional reflection deriving the upper bound on K is located in appendix 1. At low field levels equation 4 can be understood as a statement of the dissipation as a result of material resistivity. The denominator is the response of a very good conductor. The numerator describes a similar sample where we are increasing the permeability possibly by increasing the sample temperature. Equation 5, however, is only a result of solving Maxwell's equation using the simple linear magnetic equation of state,

$$\mathbf{B}=\mu\mathbf{H} \qquad [6]$$

The weakness in this model description of a ferromagnetic material is apparent when the ratio K is measured at values greater than 1. This solution is analogous to any optical reflection where the reflected amplitude is always less than or equal to the incident source.

In a good conductor the one dimensional cylindrical solutions are quite accurate for a long sensor because the fall off in fields at the coil ends are abrupt, $\frac{1}{r^4}$. Where r is the distance from the end of the coil. This rapid decrease results from the cancelation of the fields due to the out of phase induced field in the conductor. So standards are typically taken with high conductivity non magnetic materials.

MEASUREMENTS

The effects to be examined here are the reflection of an imposed time varying field on various ferromagnetic materials. In addition the transmission of a signal generated from a time varying field will also be examined. Particularly, the penetration of signal well beyond the electromagnetic skin depth in soft ferromagnetic conductors. The analysis is strictly macroscopic with the aim of determining the changes required in the application of Maxwell's equation in order to physically understand the responses. The equipment used evolved from early multi frequency eddy current instruments used on stainless weld measurements(17) where the response of minority delta ferrite and solidifying cast irons(18) were monitored for phase and magnetic transformations. The signal generation and detections system used in the current measurements is a Process Monitor IV from Casting Analysis Inc. which has three quadrature phase detectors that can provide three signal sources that operate independently. All detectors use a common master clock which maintains a uniform phase relation in time among all channels. The system can feed all three signals into either a single or multiple coils that can be detected on any three channels. The operating frequency range is from 1 Hz to 20 MHz. Typically this instrument is used for multi frequency direct inversion of calibrated eddy current data for monitoring properties over a wide temperature range such as crystal growth.

The operating software can compute the boundary value problem in the geometries that are used in the following experiments as a long solenoid and a single loop. The quadrature responses are computed for the standard and then data taken on that standard is used to compute the matrix $\mathbf{T}_i$ for each frequency, ω_i of measurement. This allows single or multiple frequency reflection measurements to be made along with transmission measurements. When taking transmission measurements the calibration uses the sample under test as the standard

or no sample with the source and receiver as close as possible. This gives a reference at a phase angle of 0^o so that measurements on the bar produce the total phase shift as referenced to 0^o or the source. The typical maximum drive are 10-20 milliampere for the reflection experiments into 12 turn coils 1.5 cm in diameter and 1.5 cm long. These coils are driven in series with a 51 ohm resistor. The sample diameter determines the local maximum for the field. All detector coils are terminated with a 51 ohm resistor to ground. The detector coils are the same construction as the probe drive coils. The current levels are set at least an order of magnitude below where we cannot detect non linear components in high purity well annealed iron when two different frequencies are used to drive the source. The linear behavior of the system acting on copper is confirmed experimentally in data taking with increasing current inputs showing a well behaved response as shown in figure 4. The behavior for iron is different with a response increasing monotonically with drive level in the same figure.

Simple Cylindrical Boundary Value Reflection Experiment and Analysis

The first experiment is a simple reflection measurement in the cylindrical geometry for a set of standard materials when the source and sensor are the same, show the non classical behavior of the detected amplitude to the applied signal. For a magnetic material with $\mu > 1$ the value of $\mathbf{K}$ should be less than 1, however, the two magnetic materials measured show values between 22 and 35. This is a very large error, greater than 2000% for the application of a simple constitutive relation, $\mathbf{B} = \mu\mathbf{H}$.

The simplest reflection experimental data is recorded in figure 4 which shows the signal for 3 samples at two different frequencies while the source drive level is increased. The key point to take from this data is that for soft ferromagnetic conductors and insulators there is measured a significant signal energy above the applied level. As shown previously, it is not possible to get a result found in figures 3 or 4 by varying μ in the complex plane. There is also no apparent resonances detected in the frequency range as shown in figure 4.

The apparent enhanced level measured at the applied frequency is not a peaked resonance as one would find in a oscillator associated with a local physical property; because if the frequency is decreased, there will be a slow increase in the amplitude. By using $\mathbf{B} = \mu\mathbf{H}$ there is not a way to compute a return amplitude greater than 1. Since ferromagnetism is a quantum mechanical phenomenon there is not any reason to assume that the macroscopic field should be proportional to the applied induction. These large signals also indicate we do not have accurate knowledge of the spatial distribution of the fields within the cylinder.

Radial Scale Independent Measurement of Long Solenoidal Reflection

To gain more understanding of the difference of a ferromagnet such as iron to a simple conductor such as copper in the response, it is easy to remove the radial scale dependence from the problem of figure 3a to get a material response that is independent of the radius of the sample for a known applied field. If the material behaves as a simple reflector with Joule dissipation of the induced currents this value should be independent of the sample's radius. The boundary value problem for the continuity of the electric field, $\mathbf{E}$ and the magnetic induction $\mathbf{H}$ result in a pair of equation at the boundary of a homogenous cylinder radius, r, where k_o is the free space propagation vector.

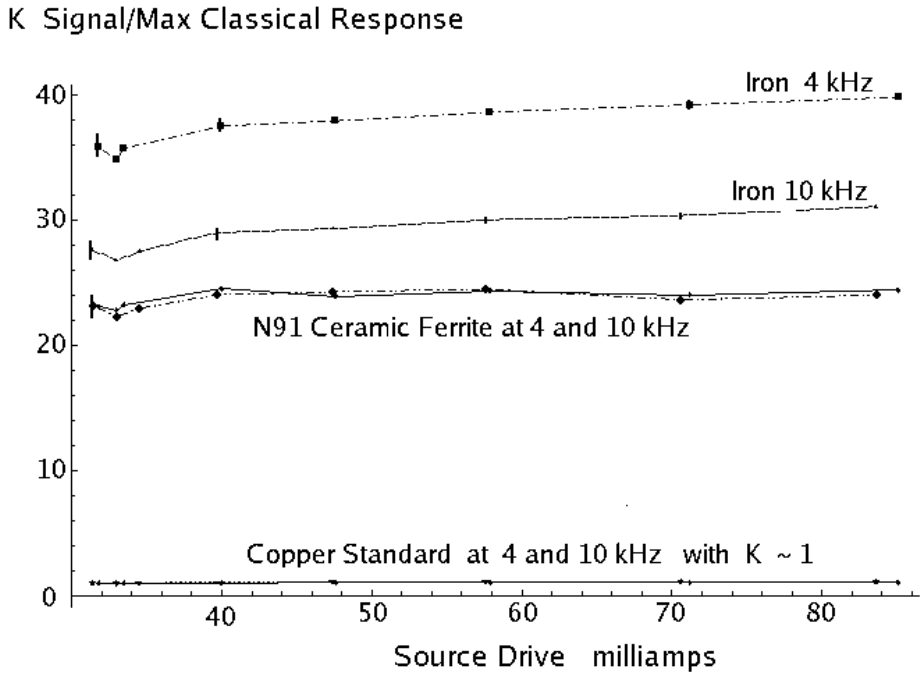

FIG. 4: **Single sensor measurements of reflected eddy current response in copper, iron and a NiZn ferrite. The key feature is that the ferromagnetic samples all have K $\gg$ 1. In the case of iron this value approaches 40. The iron in this case was of 99.99 % purity and held for greater than 30 days at 1050 C^o in flowing hydrogen and then furnace cooled. This was to reduce the interstitial content. Iron differs from the other samples in that there is a signal increase as a function of drive current. This is not the case for copper or the ferrite. This nonlinearity is also not predicted by the classical modeling in the boundary value problem. The variations at low current levels are caused by low signal level for the copper standard resulting in reduced precision. In this experiment field levels range up from 10^{-7} Tesla.**

$$AJ_1(k_o r) + BY_1(k_o r) = CI_1(kr) \qquad [7]$$

$$\frac{1}{\mu_o}(AJ'_1(k_o r) + BY'_1(k_o r)) = \frac{C}{\mu} I'_1(kr) \qquad [8]$$

If the source coil has a radius, r_c, with a source field $AJ_1(k_o r)$ we can consider the field at the surface of the cylinder is normalized by the ratio $J_1(k_o r)/J_1(k_o r_c)$ and similarly the response from the cylinder is normalized by the ratio $Y_1(k_o r_c)/Y_1(k_o r)$. The measured responses, S, amplitude is then found in the scale independent form, S_n as:

$$S_n = S\frac{J_1(k_o r_c)Y_1(k_o r)}{J_1(k_o r)Y_1(k_o r_c)} \qquad [9]$$

Taking data on some annealed low carbon steel and copper of different radii at 10khz illustrates the difference in the materials' responses.

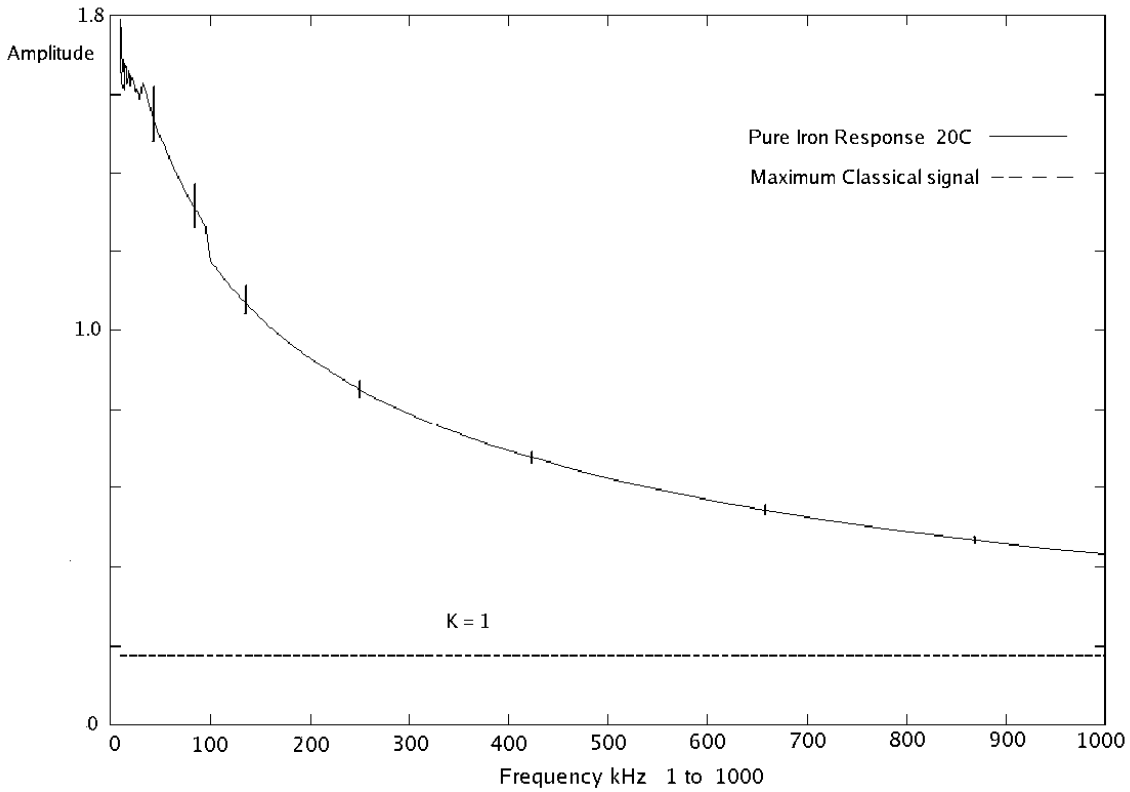

FIG. 5: **Single sensor measurements of amplitude plotted as a function of frequency in high purity iron. This graph is composed of three separately calibrated sweeps and joined together to cover the frequency range. The offsets can be seen from joining data together. The noise at low frequencies is due to less resolution for the calibration measurement on copper which is used to normalize the data to assembling the sweep on one scale.**

Table 2: Scale Independent Response with A Long Solenoid for Copper and hot rolled 1018 steel, 10kHz coil 7.85mm Radius. The measured signals in Copper fall off very fast as the radius is reduced, where as the signals actually grow in the hot rolled 1020 steel as the radius was reduce. The steel was used over pure iron is simply as a cost consideration of wasting pure iron by turning it down. The induction response of hot rolled mill annealed low carbon steel is very close to that of pure iron. The ferromagnetic properties of the iron dominate the contributions from the widely distributed cementite precipitates.

Cu Radius mm	S ± .007	S_n	Fe Radius mm	S ± .007	S_n
4.75	.319	**.87**	5.85	2.00	**3.60**
4.25	.263	**.89**	4.85	1.54	**4.03**
1.55	.027	**.7**	3.95	1.276	**5.04**
			2.65	.888	**7.79**

The main feature of table 2 is that copper's response is nearly independent of radius and the signal for the iron data is large and inversely proportional to radius. The result is an

increasing signal with reduction of radius where the ohmic loss effects have already been corrected as a function of radius.

The practical coupling of fields to ferrous cores in transformer design illustrates some problems for weak time dependent field when increasing the surface area relative to volume. It is not apparent that the traditional explanation of eddy current losses play much of a role in this optimization for more area per unit volume in a ferrous core for weak fields.

Saturation Effects on Transmission and Local Signal Level

One simple experiment that can be performed in measuring the locally reflected field from a cylindrical sample is to apply an axial static magnetic field of a few hundred gauss from a ceramic permanent magnetic with a central hole in which a sample can be placed with a coaxial coil, figure 3a. This has the main effect of removing a significant fraction of MDB and aligning the static magnetization within the material. The effect on the local signal shows a large difference in the soft magnetic materials. The locally measured signal and the responses with and without a static axial magnetic field are listed below. **Table 3: Effect of static magnetic field on the reflection for 50 kHz signal. Errors in phase measurement $\pm.02^o$ and in amplitude measurements $\pm.002$.**

Material	**phase ϕ**	**change in phase**	**% amplitude reduction**
Fe	-39.7	-35	87.5%
Ni	-84	-63	30%
Co	-81	-29	27.5%
Ferrite N91	-2.7	+1.5	96.2%

The phase data shows the metals Ni and Co with the saturating fields decrease with partial saturation. The Ni and Co are from machined bar stock and not annealed whereas the Fe sample is a well annealed specimen with very low interstitial impurity content. For a simple conductor the phase angles fall between $-90^o > \phi > -180^o$ whereas for a ferromagnetic insulator like N91 the phase angle will approach 0^o or $S_m = (amplitude, 0)$ for a response vector. The static **B** field is not quite strong enough to push the phase angle response of Fe to values as low as -90^o. The NiZn, N91, ferrite is the softest of the materials and whose amplitude is greatly effected, but its phase is driven towards 0^o which is indicative of a more highly permeable insulating material response for a classically describe magnetic material. The iron and the ferrite response are well beyond what one would calculate as the limiting response for a classical reflection without the static field. With the static field the phase angles fall into better agreement with a classical analysis. The result of minimization of MDB area or immobilizing MDB on microstructural features from cold work acts similarly by removing a significant portion of the nonclassical response.

PROPAGATING WEAK FIELD MEASUREMENTS

For propagating fields our first measurements are for weak time varying fields with long free space wavelengths that will act as a small perturbation on the iron. We are within a small fraction of the free space wavelength at the source field for the entire frequency range

being examined. The dispersion of the components that produce the measured excesses in the reflection responses may allow the individual sources and propagation modes to be isolated and identified. By scanning the displacement of the receiver as well as the frequency of the source, the overlapping effects that occur with a single driven sensor/receiver can be partially lifted.

Calibrating the transmission standards is much simpler because it can be a differential measurement from the position of closest approach of the source and receiver normalized to a signal vector $S = (1, 0)$. The first component representing the magnitude of the component in phase with the source and the second component is the amplitude of the signal that is phase shifted -90^o to the source. The zero point is established by removing the drive signal from the source. This allows the differential phase change to be acquired accurately with displacement. An absolute calibration can be made by removing the medium and measuring the source field directly as is done in the single sensor measurement. The amplitude responses are scaled to the normalized source amplitude at the closest approach. This allows a direct measurement of the fields decay as a function of displacement.

In the transmission experiments, figure 3b, the coil drives are typically 30 milliampere into 10 turn coil 1.3 cm in diameter and .9 cm long, driven through a 10 ohm series resistor. The sample diameter determines the local maximum for the field which can be easily computed. The detector coil is the same as the source coil and is terminated with a 51 ohm resistor to ground and it feeds a transformer input on the Process Monitor IV. In translation measurements for the extraction of the dispersion curves Process Monitor IV steps the probe down the bar taking readings every .05 mm while running at a single frequency for each scan. When selecting a frequency to work at in the transmission mode a frequency sweep should be made with the source off to determine if there are any extraneous signal sources being sensed.

First Transmission Measurement

From the literature it is known that induction formed propagating fields in iron and steels exist(7). Also we have a great deal of data(19) on the high temperature measurements of steels with a single probe which shows a significant enhancement of the field levels above what we measure at room temperature. An example of this is shown in figure 6. The other features of the high temperature data are the constant phase value as one approaches the Curie point and the decreasing noise level detected in the large reflected response. In the example in figure 6 the signal increase is by a factor or 6 moving to the Curie point. The phase drops at the Curie point to a value expected of a conductor at above 770^oC.

The question posed here is whether transmission will be possible in a region where the steel is raised above the Curie point? This transmission experiment depends on two processes, first is generating the field and the second is the role the medium plays in its motion. This immediately would reveal whether the signal could survive in a region of no permanent magnetic moment but a spin wave population and no magnetic domain structure. If it did traverse that region then it answered one question about the necessary medium required for transmission of the signal. This first experiment was done on a 4.7 mm diameter rod 1018 hot rolled steel. The coils were 11 turns mounted on water cooled copper mono turn rings and 8 mm long. The calibration was based on the source and receiver coils empty and far removed for a zero point. Then the coils brought close together axially for taking the 0^o phase and amplitude reference. So that all subsequent measurements are referred to these

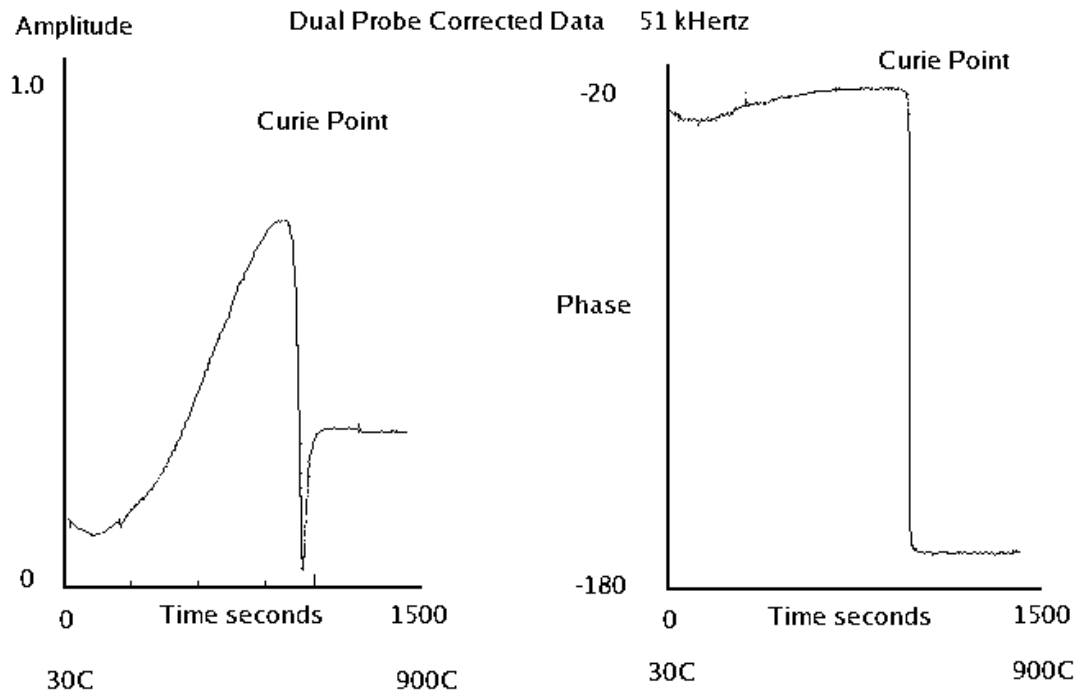

FIG. 6: **Single sensor on iron at 51 kHz, heated from 30 C to > 900 C reflected amplitude response on the 0^o axis. Data taken on a Process Monitor II in a low carbon steel.**

measurements and the phase delays are absolute and caused by the material.

The transmission data for phase and amplitude with the heated center are shown in figure 7 and 8 respectively. In the vicinity of the Curie point there was a rapid increase in the phase delay along with a steep increase in response. Then as the center region passes through the Curie point the transmission level abruptly drops, not to zero, but to value that stills shows a transmission response double that of the room temperature value. This response is made up of a combination of the gain in the heated rod below the Curie point and the loss in the region above the Curie point. The phase delay suffers a significant reduction with the section above the Curie temperatures. The transition through the Curie point arrests a portion of the propagating field but from a classical EM analysis the attenuation is too weak and the phase response is of the wrong sign. That is if an axial induction at 10 kHz is impressed on a conductor it is rapidly attenuated on the order of 1 mm and is phase is significantly delayed and not advanced. Where as the single coil heating experiment of figure 6 shows nothing unusual and differing from a classical EM response above the Curie point. Generation of the excess signals seen below the Curie point both in the transmission and single sensor data are not explained by a classical analysis.

The heating for this particular data was done with a propane flame and not an electric furnace. If an electric furnace is used the results are much more complex depending on the content of ripple in a DC supply or an AC power source is used because this induces a nonlinear interactions with the time varying heating field from the heating elements. If you were to replace the heat source with a local transverse strong static magnetic field at the

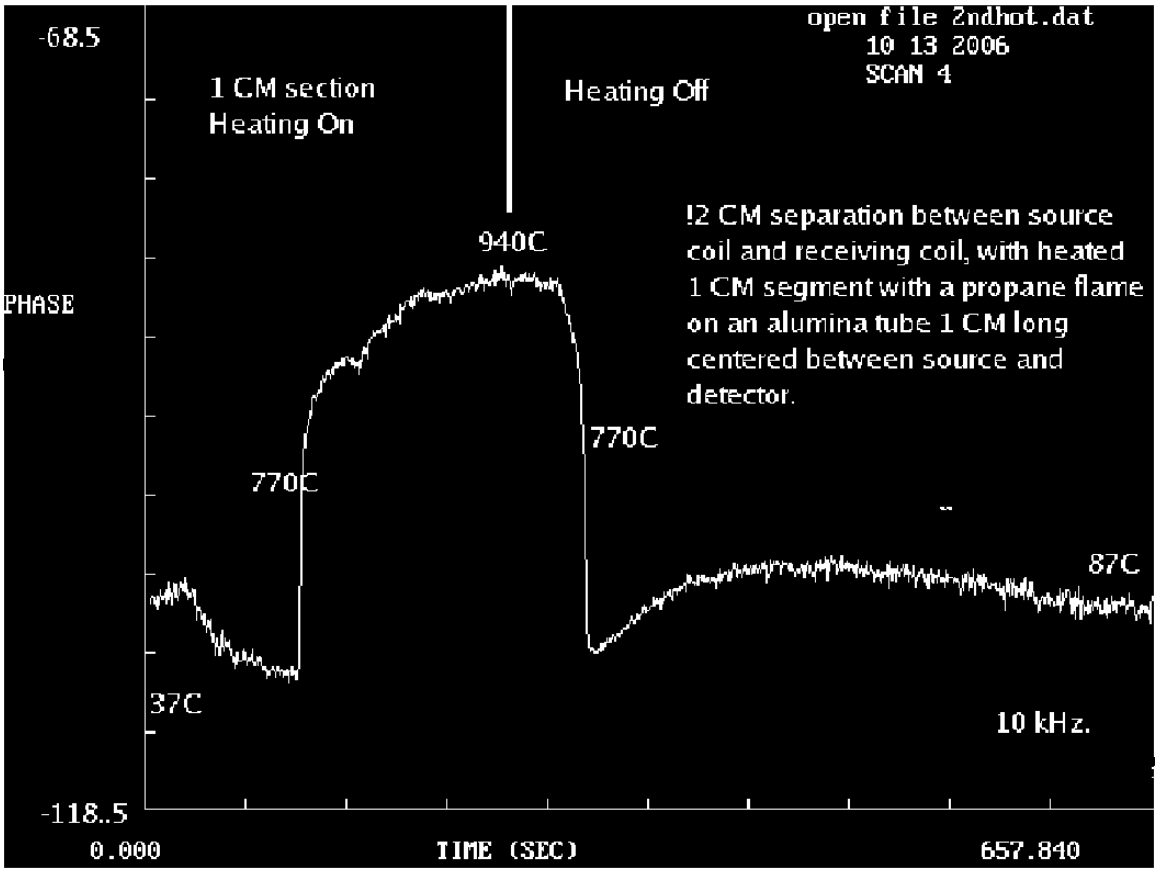

FIG. 7: **The phase response of the transmission of 10 kHz over 12 cm through a hot zone of 1 cm through a 1018 steel rod. The sample starts at 37C and is heated by flame to 940C and allowed to cool to 87C. The geometry is similar to figure 3b.**

center of the bar little change is measured.

Transmission and Dispersion Curves

The transmission measurement is a very useful experiment because if a resolvable field as a function of the source frequency can be identified with a measurable phase-distance relationship then a dispersion curve for that field can be constructed. These measurements were taken in a 1018 hot rolled 12.7 mm diameter steel rod 69 cm long with the measurements done at 20^{o}C. This material was selected because it is inexpensive and essentially well annealed iron with a low concentration of cementite precipitates, very little carbon in solution and annealed by the slow loss of residual heat stored in the large coil formed from a single billet after hot rolling. It suffers only a mild straightening operation with its *wüstite* patina in tack. Because of the heating and rolling in air and the visible oxidation there will be a surface decarburization band which will leave a relatively pure iron just below the oxide.

From the linear displacement of the receiving probe two well resolved fields were observer and one poorly resolved field with sample raw data from 3 of the 15 scan taken shown in figures 9 and 10. Field 1 below 30 kHz is possible acoustical field but it is heavily damped with a detectable to a range of 4 cm and estimated velocity of 4 $\times 10^3$ m/s is shown in figure

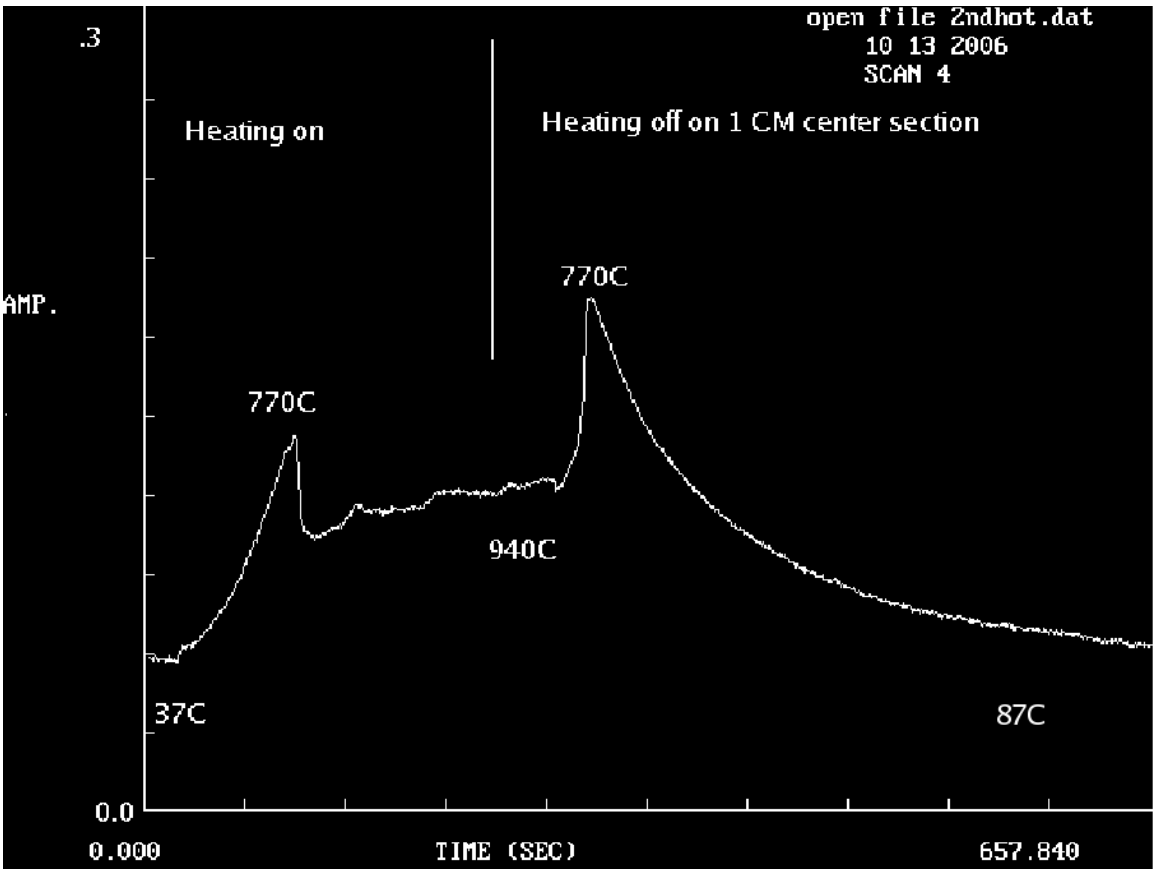

FIG. 8: **The amplitude response of the transmission of 10 kHz over 12 cm through a hot zone of 1 cm through a 1018 steel rod. The sample starts at 37C and is heated by flame to 940C and allowed to cool 87C. The geometry is similar to figure 3b and the source and receiver coils were cool. The asymmetry in the response as the flame is removed only represents the cumulative heating of the rod as the heat diffuses outward from the center changing the gain characteristics.**

11. Because is heavily damped and so short range it is not a candidate for a stress wave. There are not enough data to classify this short range field at this time. This field 1 is only resolved at the lower frequencies and it could not be resolved above 30 kHz.

The next dispersion curve for field 2 emerging resolvable with field 1. is detectable to 2 MHz, figures 11,13 and 14. This field has a parabolic dependence consistent with the field carrier having a mass. Its computed its phase velocity one needs to assume a band structure and one can compute and effective mass for the carrier as 2.56×10^{-39}kg ($2.7 \times 10^{-9} m_e$). This field was not expected in a room temperature poly crystalline steel when the effective mass computed neutron scattering data(20) to produce values of 1.18×10^{-31}kg ($13 m_e$) for a spin wave. Its very low mass makes it a candidate for a new type of quasi particle or a highly modified band structure of the spin wave spectrum.

At higher frequencies beyond 500 kHz field 3 dominates the measurements and its amplitude grows, figure 11. This field is at the edge of being resolved at high frequencies because of its very small phase shift even though it has a large amplitude. The growth of the signal for field 3 is shown in figure 12. From the Ln plot of the dispersion curves 2 and 3 look

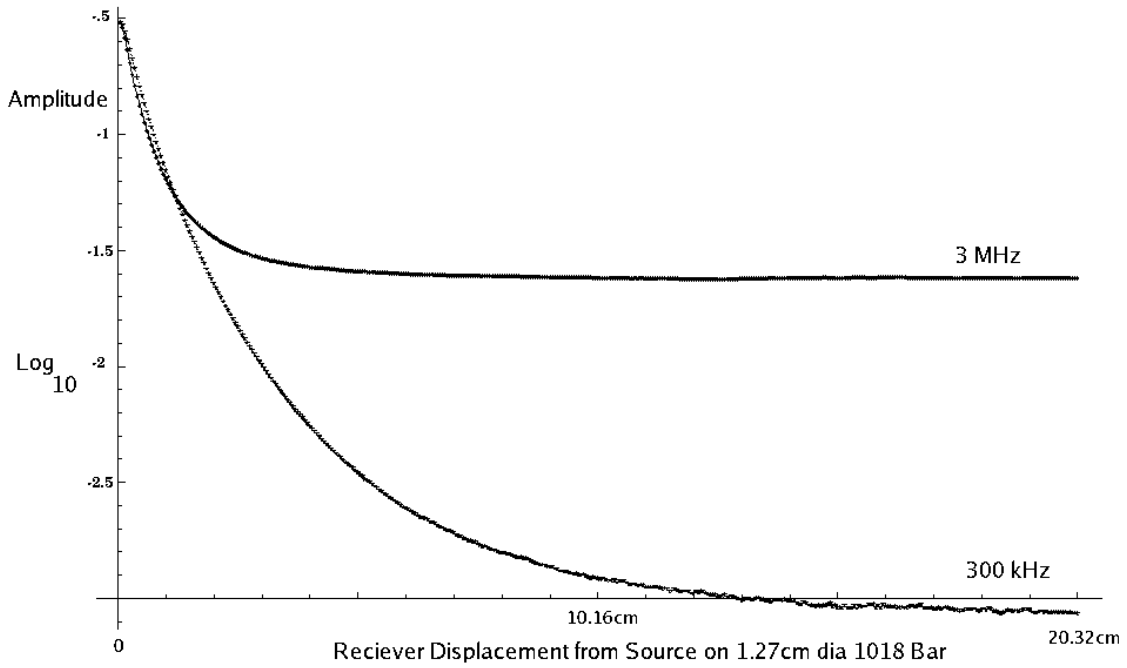

FIG. 9: Log_{10} **Amplitude of a 300 kHz and 3 MHz Signal verses separation from source. Displacement amplitude sample data above is one of a set of 15 scans at frequencies from 3 kHz to 3 MHz. The data was used to construct the transmission response graph in figure 10.**

related.

MECHANISMS AND SPECTRA

To begin the discussion the easiest field to consider first is field 2. The applied induction,$\mathbf{H}(\omega_i)$, will lift the phase degeneracy of the group of spin waves via the contribution to the Hamiltonian, H_{int}.

$$H_{int} = -\mathbf{m}(t) \bullet \mathbf{B}(t) \qquad [10]$$

If this is true then a collection of relatively short wave length spin waves get transformed in to some very long wave length spin waves. Extracting the dispersion curve for this data we get the set of equations:

The zero field dispersion curve generated from neutron scattering(20) and all energies are in units of joules and wave vectors are in $meters^{-1}$:

$$E_{m=0} = 4.5 \times 10^{-40}\mathbf{q}^2 J \qquad [11]$$

The dispersion curves extracted from figure 13 is:

$$E_{m=+1} = -\epsilon + 2.2 \times 10^{-30}\mathbf{q}^2 J, \mathbf{q} < nullpoint \qquad [12]$$

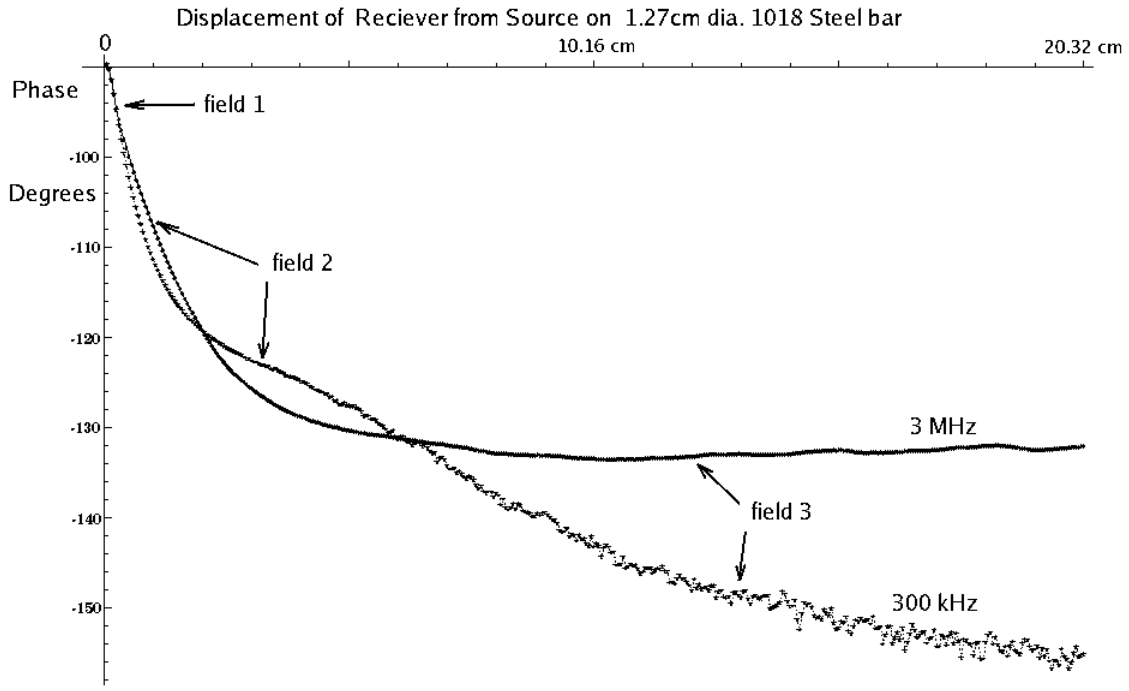

FIG. 10: **Phase of a 300 kHz and 3 MHz Signal verses separation from source in degrees. This is one of a set of 15 scans made from which the phase data and distance information was gathered. Data from these phase scans were used to construct the three dispersion curves in figure 11**

$$E_{m=+1} = +\epsilon - 2.2 \times 10^{-30}\mathbf{q}^2 J, \mathbf{q} > nullpoint \quad [13]$$

The m=-1 curve is estimated to be the flipped version of the m=-1 and it does not disagree significantly with the data of figure 11.

$$E_{m=-1} = \epsilon - 2.2 \times 10^{-30}\mathbf{q}^2 J, \mathbf{q} < nullpoint \quad [14]$$

$$E_{m=-1} = \epsilon - 2.2 \times 10^{-30}\mathbf{q}^2 J, \mathbf{q} > nullpoint \quad [15]$$

Where m=1 represents the in phase branch and m=-1 is the 180^o branch. The m=0 branch does not have its phase degeneracy lifted so that it must follow the zero field data line. The null point is the point at which all three bands would cross as mathematical functions. Since this would create a degeneracy and not be energetically realistic, the extracted dispersion curves take on the above form.

Allowed States

But with these long wave length spin waves, there is a density of state problem. Mainly is there a state available to support them? Taking the data from the dispersion curve 2 to estimate the size of the sample required to support the state a coarse estimate can be done

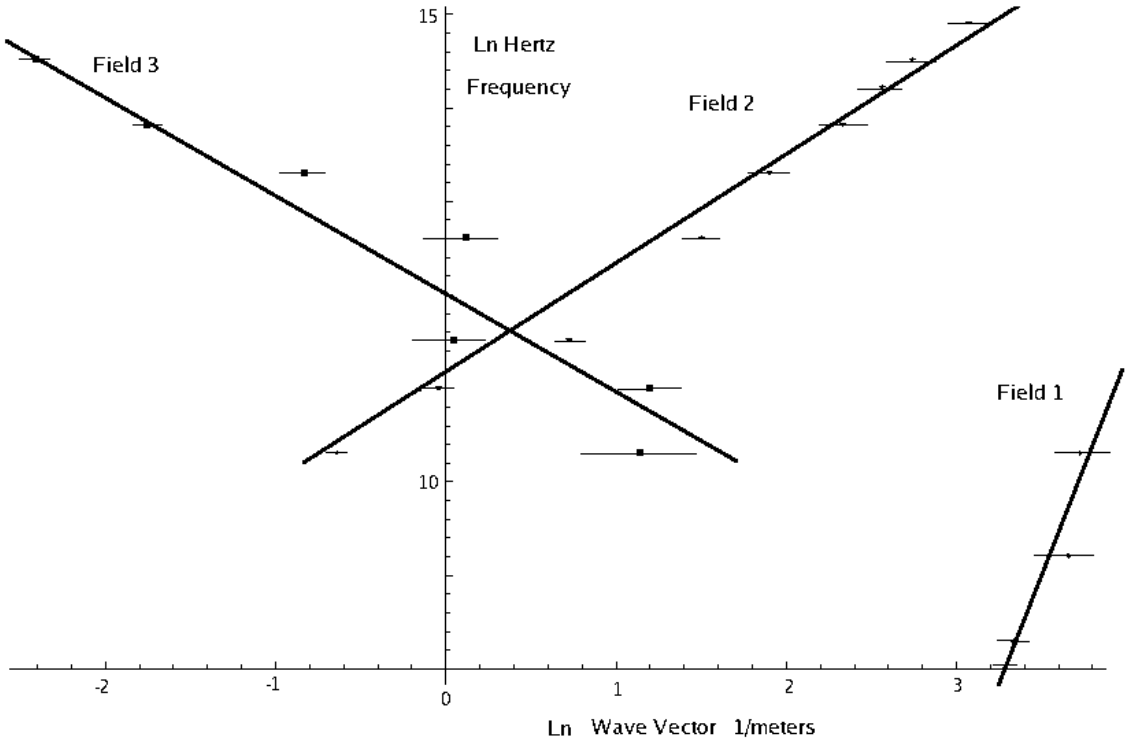

FIG. 11: **To fit the three dispersion curves on a single graph a natural Log-Log plot in frequency for the vertical scale and propagation vector K in 1/meters. Field 1 has a velocity sound and is only seen below 30 kHz. Field 2 has a computed effective mass of 2.59×10^{-39} kg ($2.7 \times 10^{-9} m_e$). Field 3 dominates above 500 kHz and rolls off very slowly with some phase variations indicating interference effects.**

where the second derivative approximates the exact expression for the BELC which is the fraction in equation 16.

$$\frac{\partial^2 E_k}{\partial k^2} = \frac{E_{n-1} + E_{n+1} - 2E_n}{\triangle k^2} \qquad [16]$$

The quantity $\triangle k^2$ is dependent on the characteristic volume of the state in which the spin wave population is defined which has a linear dimension, Λ.

$$\triangle k^2 = \frac{4\pi^2}{\Lambda^2} \qquad [17]$$

The energy jump is approximated by the measured ϵ:

$$E_{n-1} + E_{n+1} - 2E_n = 2\epsilon \qquad [18]$$

$$\frac{\partial^2 E_k}{\partial k^2} = \frac{\epsilon \Lambda^2}{2\pi^2} \qquad [19]$$

where the size is:

$$\Lambda = \pi \sqrt{2 \frac{1}{\epsilon} \frac{\partial^2 E_k}{\partial k^2}} \qquad [20]$$

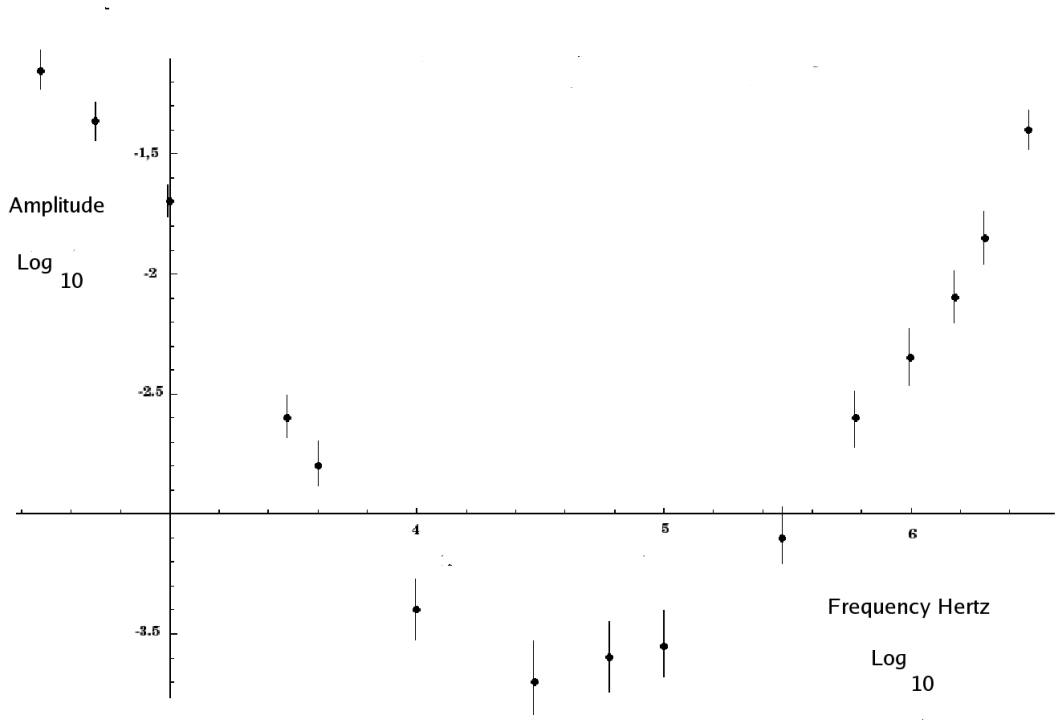

FIG. 12: Log_{10} **Amplitude verse** Log_{10} **Frequency for Long Range Field at 20.32 cm from source. This data has a practical application in that for induction heating one would want to minimize the propagated energy loses and that would have a minimum for this particular steel at about 30 kHz. This minimum is where induction heating of steel is found to be most efficient below the Curie point.**

The size, Λ can be solved for from equation 20 and using $\epsilon = 3.9 \times 10^{-29}$J and the second derivative of equation 12 results is a size of 36cm. This size indicates a single state along the axis of the bar which will call the z-axis for $+\mathbf{q}_z$ and $-\mathbf{q}_z$. Now this is beginning to look like a BELC with one available low energy state for each direction of propagation, if they can be populated. This can be summarized in the schematic in figure 15 showing 6 allowed states for the BELC

A major feature of this schematic is the null point. It represents where BELC like behavior should vanish and is the contention here that the minimum in the data in figure 12 represents this minimum amplitude in the transmission. The null points dependencies on the drive amplitude and size have not as yet been explored. In this data the depth of zero frequency intercept is, ϵ. The null point occurs at approximately 30 kHz for these measurements resulting in an $\epsilon = -3.9 \times 10^{-29}$J. At the null point the m=+1 and m=-1 branches cannot cross as the m=-1 branch must remain the high energy branch, instead the branches are connected as seen in the inset of figure 15. Similarly if states are formed from varying strength source field within the steel the measurements will reflect a distribution of bands and intersecting null points.

Field 2 that has a propagating magnetic moment, a small effective mass a relatively high velocity and if it is made of coherent collection spin waves then it is behaving as Bose-Einstein like condensation (BELC). This second field which falls off rapidly is heavily attenuated with

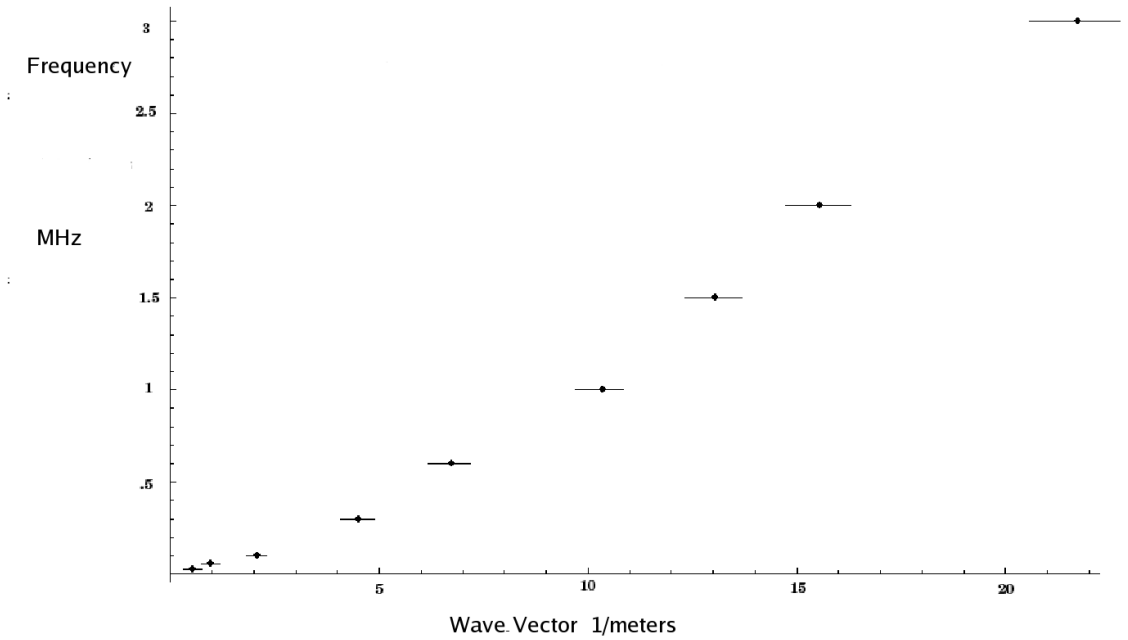

FIG. 13: **Field 2 plotted showing a parabolic relation between frequency and propagation vector. This field was found to span the entire range from 3 kHz to 3 MHz.**

increasing frequency. The fall off in this third field is less than 6 db per meter estimating from the data in figure 9 for the 3 MHz signal. Data from the elevated temperature in the bar's middle indicates the second field is arrested at the Curie temperature and the third field propagates through the zone above the Curie point and is detected. This is inferred from the phase increase because of this transition region and the lower dispersion that is found for the third field.

Polarization of $\mathbf{q}(\mathbf{m}, \omega)$

Nothing has been said to this point on the relation of the propagation vector to the time dependent magnetization polarization of the spin wave, $\mathbf{q}(\mathbf{m}, \omega)$ on the two active branches of the low energy dispersion traces. Assuming three circular polarization axis with either right or left handed symmetry gives 18 possible states in combination with three principal axis for the propagation vector. With respect to any axis selected by the applied field 4 of the 6 possible polarizations will have a projection on the applied fields axis for all of the propagation vector directions. That means that only $\frac{2}{3}$ of the available spin waves states will be effected by a time dependent induction. This means that the BELC will contain all propagation directions and this is not disputed in the way field 2 decays. The axially parallel component of polarization should show excellent propagation characteristic down the bar, where as the transverse polarizations should be extinguished quickly unless the rate of reoccupation driven from the thermal and non thermal spin wave pool is efficient. The polarization distribution may explain the filtering effect of the region of material held above the Curie point where the $\mathbf{q}_x$ or $\mathbf{q}_y$ population produces no gain in this region and its

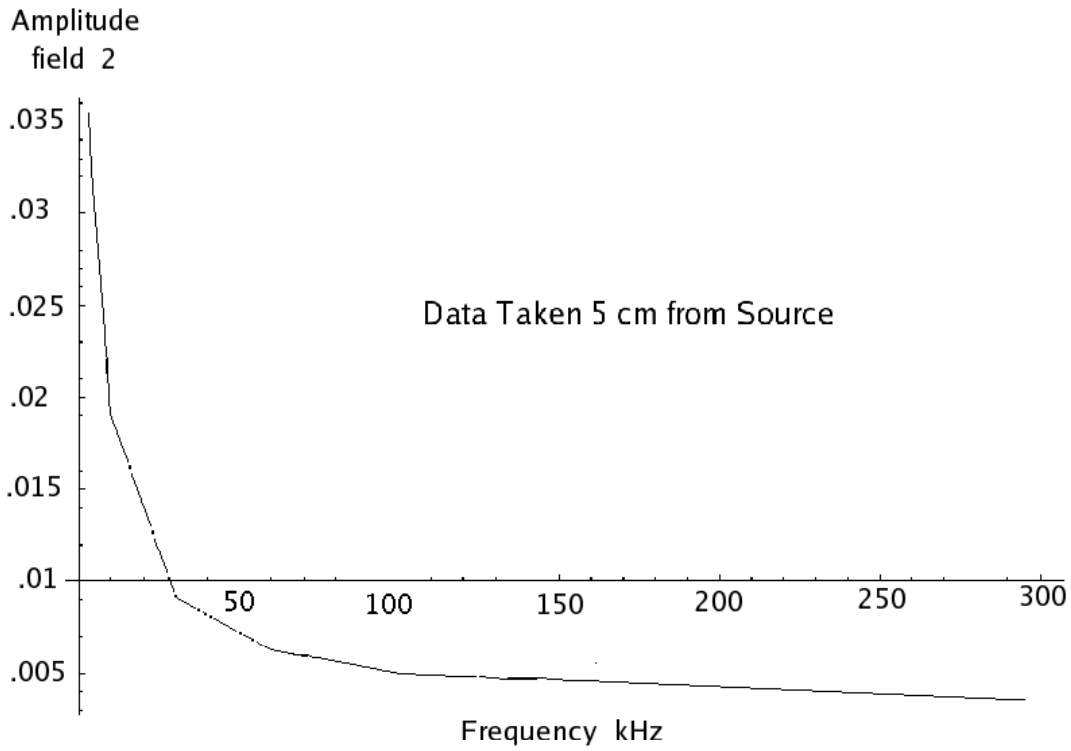

FIG. 14: **The amplitude of the signal in field 2 falls off rapidly with frequency. The receiver is placed at 5 cm from the source. At high frequency the response from field 3 is building and beginning to dominate the signal above 500 kHz.**

contribution is simply reduced by spreading isotropically within the bar. Whereas the $\mathbf{q}_z$ simply traverses the region. The phase shift fits this picture as it appears that field 3 from the extended branch has the characteristics of $\mathbf{q}_z$ with a phase delay that is significantly lower than that for field 2 which falls off at greater than $\frac{1}{r^2}$. The source of this phase delay between the two sections of the dispersion curve of the propagation vector needs to explored and computed. Because if the the MDB motion is a non thermal source for these states the near surface domain boundaries are constrained relative to the boundaries well within the material to effect the distribution of radiated spin waves. From the simple experiments effecting the MDB density or mobility is evident their active is the strongest contribution to the pumping of the BELC state. The concentration of the signal in field 3 makes it difficult to assume that the $\mathbf{q}$ are isotropically distributed in all directions. The parallel population just maybe favored on the basis their direction allows for a longer lived state because of not annihilating at a free surface. There are other experimental geometries more suited to testing these concepts. It is possible to gather data on these properties by scattering different orientation of created BELC and measure the distribution of product states to gain this polarization information.

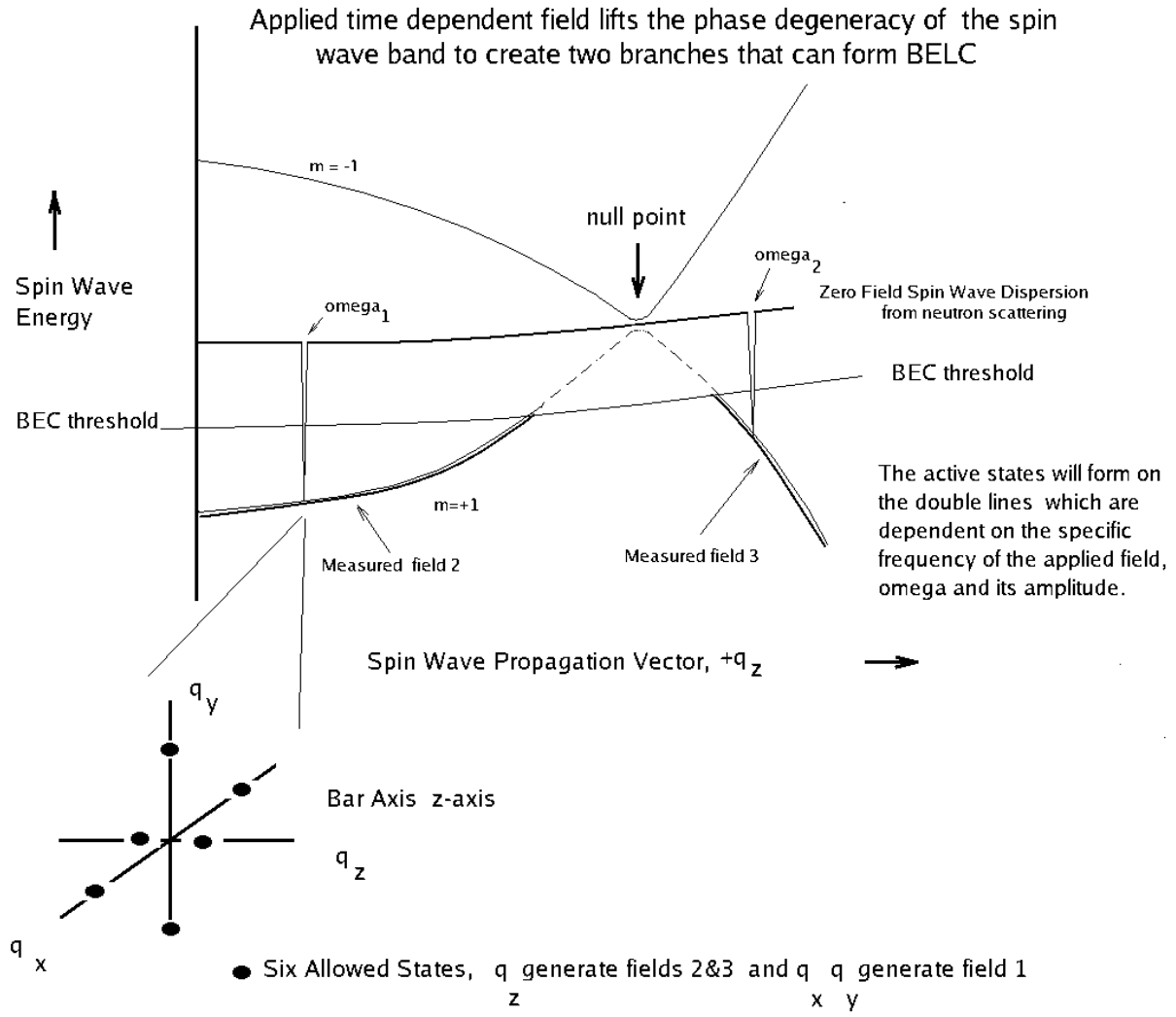

FIG. 15: **Trace of the set of dagger like states on the spherical shell of states at the applied frequency breaks down into 6 states in q-space in the limit of the wavelength expansion of the spin-wave. The linear trace shown above is a 2-D schematic of the $+\mathbf{q}_z$ states. This limited set of states confers the BEC like properties on the spin waves by reducing the near continuum to a single state for each propagation direction of 3-space. Two schematic representation of states at ω_1 and ω_2 in bands m=+1 and m=-1 show the structure maintaining m=+1 as the branch capable of forming a BECL. This is not an accurate map of the energy.**

Field 1

The source of field 1 using this BELC model is the m=-1 population of $\pm\mathbf{q}_x$ and $\pm\mathbf{q}_y$ states. The application of a time dependent z-axis field will couple into the magnetization of the orthogonal spin waves because the magnetization of the spin waves are two dimension and the three polarization cover all directions. This field 1 provides the large field strength in the single coil measurements because they are localized at the coil and not propagating

down the bar and therefore states all active and not just the $\pm\mathbf{q}_z$ axially propagating down the bar. If this state was not strong because it is so short range it could not have been resolved in the displacement dispersion measurements. The cut off at 30kHz maybe nothing more than an unresolved overlap into fields 2 and 3.

Implications of the Dispersion Properties

Estimating $< H_{int} >$ for the propagating field tests how this energy compares with the measured ϵ. At the surface of the bar the field is estimated $\mathbf{B}(t) = 3 \times 10^{-}5$ Tesla. This is the peak field averaged along length of the empty inductor. Taking $\frac{1}{2}$ for the time average and the exponential field average in the materials produces a factor of .217 and a mean field of 6×10^{-6} Tesla. This yields a value for $< \mathbf{H}_{int} >= 6.0x10^{-29}$ J . This number is not too different than what was extracted from band structure schematic of the intersecting dispersion curves.

High temperature BELC have been detected in spin wave systems that are laser pumped(21). The expression for the transition temperature(22) for the BEC is :

$$T_{BEC} = \frac{\mathbf{n}^{2/3}}{m} \frac{2\pi\hbar^2}{k_b \zeta^{\frac{2}{3}}(\frac{3}{2})} \qquad [21]$$

Where $\mathbf{n}$ is the number of spin waves, m is the mass, ζ is the zeta function. To have a $T_{BEC} = 770^o$C one only need an occupation number of greater than $\mathbf{n} = 1.97 \times 10^{12}$ and at 23^oC the required density is 2.93×10^{11} . These numbers compared to what is available at and above room temperature with an applied field. Using the energy gap from figure 15 of 3.9×10^{-29} J yields a thermal density of spin waves of 1.06×10^8 at 23^oC and 3.78×10^8 at 770^o C. This indicates that forming BEC at high temperatures is only favorable if you pump the state with a non thermal source of spin waves to supply the state. The non thermal sources from the current driven processes and radiation from magnetic domain motion, figure 2, particularly favor iron because of the split band structure intersecting the Fermi surface.

Spectroscopy of the BELC and Induction Analysis

The total Hamiltonian of a BELC state is made up of at least two parts, the number of spin waves in the state $n(\omega_i)$ and their interaction with the applied induction, equation 10. This is the fundamental difference to a BEC as there is a time dependence associated with the state. The easiest way to explore this is with a perturbation and the simplest perturbation is a second perturbing BELC where we can changes it level. Going back to figure 3b of our transmission experiment we will change the geometry slightly and replace the heat injected into the center of the bar to a low frequency field ω_2 with a time dependent field $\mathbf{H}(\omega_2 t)$. A coil of the same type will be used to inject the center field. By displacing the two fields by a 5 centimeters we are insuring that we do not have a direct superposition of our two applied fields.

Our original field injectable at the end will be ω_1 driven at the same levels $\mathbf{H}(\omega_1 t)$ of our transmission experiments. Where $\omega_2 \ll \omega_1$ and $|H(\omega_2)| > |H(\omega_1)|$. The spacing separation between the source and the receiver is set a 10 cm. As the field level $H(\omega_2)$ is increased two state emerge the strongest being $|\omega_1 - 2\omega_2 >$ followed by $|\omega_1 + 2\omega_2 >$ and if the field level is increased a little more another pair of states develop with the strongest being $|\omega_1 + \omega_2 >$

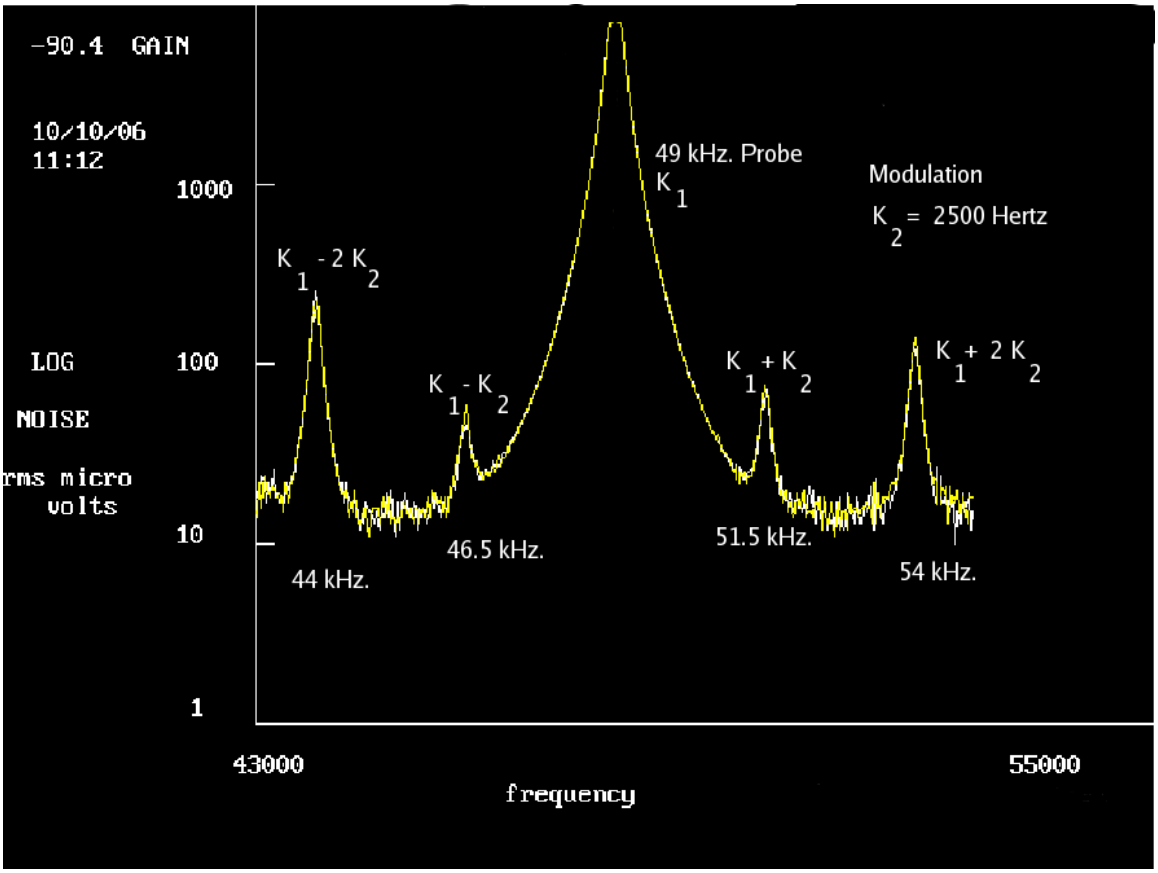

FIG. 16: **The 4 principal transitions observed when two BELCs over lap.** K_1 **is the wave vector for the weaker probe field** ω_1 **and** K_2 **is the wave vector for the stronger drive field** ω_2 **injected at the center of the bar. All signal are detected at the other end of the bar that is 10 cm section of the bar of the same material used in finding the dispersion curves. The third channel of the Process Monitor IV is used as a swept detector to provide the spectrum.**

followed by $|\omega_1 - \omega_2 >$. At this stage the original probe field $|\omega_1 >$ has managed a gain in amplitude of about 4%. A spectra of these are shown in figure 16.

If you keep increasing the drive level of ω_2 you generate a spectral comb of states $|\omega_1 \pm n\omega_2 >$ where n is an integer. The even number states and odd number states differ in how the transitions alter the polarization of the magnetization relative to the propagation vector so that apparent strengths of transitions are dependent on the geometry and the interaction that are active when measured. There are other measurement geometries more suited to working out the details of the individual transitions. Because the full set of coupling from Table 4 need to be considered as possible contributors to this spectra. These spectra and the tentative two term Hamiltonian makes the BELC unlike the BEC by the limitation on occupation numbers as higher drive levels forcing transitions to other states at high state densities. Also having multiple BELC sharing the same physical volume maybe a feature found to be usefully. **Table 4: Relative transition strengths with a probe field** ω_1 **of 49 kHz. The strengths are taken at the extrapolated limit for the injected field** ω_2 **taken to zero frequency**

Transition	**Strength % of** $<\omega_1\|\omega_1>$
$<\omega_1\|V_1\|\omega_2>$	4
$<\omega_1-2\omega_2\|V_2\|\omega_1>$	2.4
$<\omega_1+2\omega_2\|V_2\|\omega_1>$	1.4
$<\omega_1+\omega_2\|V_3\|\omega_1>$	.9
$<\omega_1-\omega_2\|V_3\|\omega_1>$	.8

There is a possible fault in this view of the spectra. In figure 4 the single coil response shows a marked non linear behavior for iron and because of this one would expect to generate the product and difference fields when two fields are superimposed on the material. In this case the introduced fields are physically displaced as is the detector. Second the spectra generated are more characteristic of momentum conserving reactions between individuals of the collective states forming their own BELC as they are then found remote at the detector. Simply having a local nonlinear field response does not account for their migration to the detector or the details of the spectra.

CONCLUSION

With the application of a transverse time dependent induction,$\mathbf{H}(\omega)$. A spherical shell of states in $\mathbf{q}(\omega)$-space has its phase degeneracy lifted. The spin waves with m=-1 and m=+1 in the limit of their expanding wave length end up with a set of six states in $\mathbf{q}$-space to allow for 6 propagating fields, $\pm\mathbf{q}_x(\omega, m=\pm1)$, $\pm\mathbf{q}_x(\omega, m=\pm1)$ and $\pm\mathbf{q}_x(\omega, m=\pm1)$. The multiplicity of the circular polarization of the spin waves allows a uniaxial induction to cause this collapse of states in all three dimensions. In terms of energy the m=+1 and m=-1 are split in each of these states. The m=0 remains and undisturbed shell of dense states in $\mathbf{q}$-space. This transformation took two equal copies of the original dense shell of states and reduced it to 12 states in the limit of the wave length expansion. The population of that original shell is left to concentrate itself in these allowed states, hence a BELC. Within a particularly state the expansion in wave lengths almost appears like a change in statistics as a variation on an early argument by Bethe(9) on coupled spin flips. It is from the correct energy map that the spectra can be interpreted. It would be helpful at this point to have polarization information along with the spectra of states to accurately characterize the couplings in the measured transitions. This data can be taken with two dimensional arrays of sources and receivers in a slightly more complex measurement geometry.

Returning to the original problem of putting Maxwell's equations into a form to handle these problems. The first thing that must be done is to replace,$\mathbf{B}=\mu\mathbf{H}$ by something which is summed over the active BELCs. A calculus for the magnetization flow and dissipation of the BELC's must be developed before the time and spatial dependent magnetization functions for the BELC can be constructed. Second question is how do you measure the value of, μ? This is important because it in part establishes the initial phase response of the material. To find μ we cannot saturate the bar with a static $\mathbf{B}$ field because that causes a change of properties. Probably the only way to determine μ is to reduce the drive levels so that a BELC is not sustained. For a macroscopic solutions one then has:

$$\mathbf{B}(t)=\mu\mathbf{H}(t)+\Sigma_i^{BELC}\mathbf{M}_i(t) \qquad [22]$$

These ideas should be useful in studying other ferromagnetic materials other than iron, which may not exhibit as many features as were found here. These effects will go along way in explaining a number of measurements made in steels over the years that were not understood. But of more general interest, the mechanics of multiple BELC activity and boson mass are topics of interest in other branches of physics. The system studied here after careful analytical development may yield more insights because of the relative ease with which experiments can be done and ideas tested.

ACKNOWLEDGEMENTS

I would like to acknowledge the careful and extensive measurement of high temperature eddy current responses in a variety of steels by Mike Bergerhouse that firmly established this problem, the discussions of signal transmission and noise through steels taken above the Curie point with Michael Wallace that gave clues to the character of the radiation source, Julian Nobel for giving me an appreciations for the concept of mass and to Steven Wallace whose patient methods of attack on problems was the example I followed. Editing to reduce these data to a readable form was generously performed by Jerry Dunn and Michael Wallace.

Appendix A: Single Homogenous Reflector

The simple case of a reflector that is a magnetic conductor or insulator can be represented by a boundary value problem where the electric field and the magnetic induction are required to be continuous across the interface. The vector potential of the source field in free space will be represented by f the reflected response will be g and the field propagating into the magnetic medium is F. The time dependence of the fields is sinusoidal, $e^{-i\omega t}$ as driven by the source. The coefficient for the field are $\mathbf{a}$, $\mathbf{b}$ and $\mathbf{c}$ to produce the three vector potentials $\mathbf{a}f$, $\mathbf{b}g$ and $\mathbf{c}F$. The electric field $\mathbf{E} = -i\omega\mathbf{A}$ and the magnetic induction $H = \frac{\nabla\times\mathbf{A}}{\mu}$. In this one dimensional representation the curl of the particular vector potential will be represented by f', g' and F'. Dividing out the time dependence the vector potential one has the relationship for the continuity for the transverse electric field:

$$\mathbf{a}f + \mathbf{b}g = \mathbf{c}F \qquad [1a]$$

similarly for the continuity of the magnetic induction:

$$\frac{\mathbf{a}f' + \mathbf{b}g'}{\mu_o} = \frac{\mathbf{c}}{\mu}F \qquad [2a]$$

We measure

$$V = \int \mathbf{E}\cdot d\mathbf{l} = -i\omega \int \mathbf{A} d\mathbf{l} \qquad [3a]$$

In the normalized form of our calibration the measured reflected field is

$$V_{normalized} = -i\omega \int \frac{\mathbf{b}g}{\mathbf{a}f} d\mathbf{l} = -i\omega\Lambda\frac{\mathbf{b}g}{\mathbf{a}f} \qquad [4a]$$

where Λ is a length Solving the continuity equations to eliminate $\mathbf{c}$ and define $\mathbf{b}$ in terms of $\mathbf{a}$.

$$\mathbf{a}\{f - \frac{\mu F}{\mu_o F'} f'\} = \mathbf{b}\{\frac{\mu F}{\mu_o F} g' - g\} \qquad [5a]$$

For simplicity taking the case of an infinite planar reflector at $x = 0$ with $f = e^{ikx}$, $g = e^{-ikx}$ and $F = e^{iKx}$ the above relation reduces to:

$$\frac{\mathbf{b}}{\mathbf{a}} = \frac{\mu k - \mu_o K}{\mu k + \mu_o K} \qquad [6a]$$

Taking in free space $k = \omega\sqrt{\epsilon\mu_o}$ and $K = \frac{i+1}{\sqrt{2}}\sqrt{\mu\sigma\omega}$ for the conducting magnetic medium. The result simplifies where d is just a constant.

$$\frac{\mathbf{b}}{\mathbf{a}} = \frac{\mu - d\mu^{.5}}{\mu + d\mu^{.5}} = \frac{\mu^{.5} - d}{\mu^{.5} + d} \qquad [7a]$$

Then in the limit of $\mu \to \infty$, $\frac{\mathbf{b}}{\mathbf{a}} \to 1$. This is true for magnetic conductor or insulator and also in the cylindrical geometry.

As a comment the two dimensional solution of a coil as a loop source surrounding a cylindrical bar taken from reference 12 equation 63 can be computed for an empty coil and one filled with one homogeneous materials. The ratio of these two integral equations can be taken in the limit of $\mu \to \infty$ to show the reflections are bounded. If the same is tried for the loop above a plane, the probe field, there is a miss print in equation 22 and 24 where the terms have not been divide by the the material permeability so that before using equation 41 this derivation has to be corrected.

BIBLIOGRAPHY

1 H. Rowland, Phil. Mag., **48** p321 (1874).

2 E.M. Terry Phys.Rev. **30**, no. 2, p133-160 (1910).

3 R.M. Borzoth, J. Appl. Phys, **8**, p.575-88, (1937).

4 H. J. Williams, R. M. Bozorth, W. Shockley, Phys. Rev. **75** p155, (1949).

5 J. Sola, US Patent, **2,694,177** Nov. 9 1954.

6 F. Brailsford, Physical Principles of Magnetism, van Nostrand, (London) 1966.

7 T.R. Schmidt, Mater. Eval. **42**, no 2 p. 225 (1984).

8 F Block, Z.Physik **61**, 206(1930);**74** p. 295 (1932).

9 A.Sommerfeld, H. Bethe Elektronentheorie der Metalle, Springer, Berlin 1933.

10 W.B. Pearson,A Handbook of Lattice Spacings and Structures of Metals and Alloys, Vol. 1, p. 908. Oxford: Pergamon Press 1967.

11 V.L. Moruzzi, J.F. Janak, A.R. Williams, Calculated Electronic Properties of Metals Pergamon Press p170 NYC 1978.

12 C.V. Dodd & W. E. Deeds J. Appl. Phys. **39**,2829 (1968).

13 L.D. Landau & E.M. Liftshitz, Electrodynamics of Continuous Media, Trans J.B. Sykes, J.S. Bell p.120 Pergamon Press, Bristol 1960.

14 R. M. Siegfried, The Reconstruction of Electrical Conductivity Profiles Using Multi-frequency Eddy Current Testing, Thesis, University of Minnesota, Mnpl. Minn. 1983

15 J.P. Wallace, J.K. Tien, J.A. Steffani, K.S. Choe J. Appl. Phys. **69** 550 (1991).

16 J.P. Wallace, US Patent, **4,651,094** March 17, 1987, col 12-14.

17 M.E. Armacanqui, Eddy Current Detection of Sensitization in Types 304 and 316 Stainless Steels. Masters Thesis Univ. Minn. 1981.

18 C.Iheagwara, A Study of Transformation Kinetics in Cast Iron and Slag using Eddy Current Technique, Masters Thesis Univ. Minn. 1982.

19 Mike Bergerhouse, private communications 1995.

20 G. Shirane, R. Nathens, O. Steinsvoll, H.A. Alperin, S.J. Pickart, Phys. Rev. Lett. **15** p146 (1965).

21 S.O.Demokritov, V.E. Demidov, O. Dzyapko, G.A. Melkov, A.A. Serga, B. Hillebrands and A.N. Slavin Nature **443**, p430 (2006).

22 L.D. Landau, E. M. Lifshitz, Statistical Physics, trans E. Peierls and R.F. Peierls, Pergamon Press,London 1958.